Direct observation of salts as micro-inclusions in the Greenland GRIP ice core

Toshimitsu SAKURAI,[1] Yoshinori IIZUKA,[1] Shinichiro HORIKAWA,[1] Sigfús JOHNSEN,[2] Dorthe DAHL-JENSEN,[2] Jørgen Peder STEFFENSEN,[2] Takeo HONDOH[1]

[1]Institute of Low Temperature Science, Hokkaido University, Sapporo 060-0819, Japan
E-mail: sakurai@lowtem.hokudai.ac.jp
[2]Niels Bohr Institute of Astronomy, Physics and Geophysics, University of Copenhagen, Juliane Maries Vej 30,
DK-2100 Copenhagen, Denmark

ABSTRACT. We provide the first direct evidence that a number of water-soluble compounds, in particular calcium sulfate ($CaSO_4 \cdot 2H_2O$) and calcium carbonate ($CaCO_3$), are present as solid, micron-sized inclusions within the Greenland GRIP ice core. The compounds are detected by two independent methods: micro-Raman spectroscopy of a solid ice sample, and energy-dispersive X-ray spectroscopy of individual inclusions remaining after sublimation. $CaSO_4 \cdot 2H_2O$ is found in abundance throughout the Holocene and the last glacial period, while $CaCO_3$ exists mainly in the glacial period ice. We also present size and spatial distributions of the micro-inclusions. These results suggest that water-soluble aerosols in the GRIP ice core are dependable proxies for past atmospheric conditions.

1. INTRODUCTION

The Earth's past environment over several hundred thousand years can be reconstructed from polar ice cores. Cores excavated at the summit of a polar ice sheet preserve insoluble aerosols in the form of dust, and water-soluble aerosols in the form of liquid or solid salt particles. Water-soluble impurities, especially acids, were until recently expected to be present mostly in liquid form (Mulvaney and others, 1988). Lately, Raman spectroscopy of micron-scale inclusions has identified salt particles in the Dome Fuji ice core from Antarctica (Ohno and others, 2005). In Holocene ice, these inclusions consisted primarily of sodium sulfate ($Na_2SO_4 \cdot 10H_2O$) and magnesium sulfate ($MgSO_4 \cdot 11H_2O$). On the other hand, calcium carbonates ($CaCO_3$, $CaCO_3 \cdot H_2O$ and $CaCO_3 \cdot 6H_2O$) were found in a shallower core from Talos Dome on the Antarctic ice sheet (Sala and others, 2008). In ice taken from the last glacial period, they consist primarily of calcium sulfate ($CaSO_4 \cdot 2H_2O$) and some nitrates (Ohno and others, 2005). The dominance of $CaSO_4 \cdot 2H_2O$ was especially pronounced in ice from the glacial maximum, which contained the highest concentration of dust and ions in the glacial cycle. Thus, at least in the Dome Fuji core, the abundances measured for these sulfates correspond well with those of the chemical compounds deduced by ion chromatography (Iizuka and others, 2008).

The borehole temperature of the Greenland Icecore Project (GRIP) ice core, excavated from the summit of the Greenland ice sheet (Johnsen and others, 1995), is far lower than the eutectic temperatures of these salt inclusions (i.e. $-0.05°C$ for $CaSO_4 \cdot 2H_2O$ (Kargel, 1991), $-1.3°C$ for $Na_2SO_4 \cdot 10H_2O$ (Usdowski and Dietzel, 1998) and $-3.9°C$ for $MgSO_4 \cdot 11H_2O$ (Genceli and others, 2007)). Their presence in solid form is therefore to be expected. The physical and chemical properties of ice formed during the last glacial cycle are similar in Greenland and Antarctic deep ice cores, but chemical impurities are more abundant in the former (GRIP Members, 1993).

Chemical impurities in the GRIP ice core have been used to show that atmospheric chemistry changed significantly between the Holocene and the last glacial period (Legrand and others, 1997). For instance, sulfate ions are more highly concentrated in glacial period ice. Calcium ions are also more abundant than sulfate ions during this period. Furthermore, in glacial period ice from the Greenland Ice Sheet Project 2 (GISP2) ice core (taken from the same summit as GRIP), ion chromatography indicates that at least 50% of calcium was in the form of $CaCO_3$, with the remainder in compounds such as $CaSO_4 \cdot 2H_2O$ (Mayewski and others, 1994). The existence of carbonate and sulfate in melted ice samples from the GRIP core has been suggested by previous studies using scanning electron microscopes and energy-dispersive X-ray spectroscopy (SEM-EDS) (Laj and others, 1997; Maggi, 1997) or X-ray diffraction (Svensson and others, 2000). The presence of these compounds as micro-inclusions in non-melted ice samples, however, has never been confirmed directly. The distinction is important, as some compounds can dissolve and react in melting ice.

In order to understand better the aerosol content of past atmospheres, we undertake a detailed analysis of the chemical composition and abundance of salt inclusions found in the GRIP ice samples. We use several techniques: optical microscopy, micro-Raman spectroscopy, SEM-EDS and ion chromatography. We measure the number density and size of micro-inclusions, and the total ion concentration of the ice samples.

2. METHODS

The GRIP ice core was recovered at the highest point in central Greenland ($72.6°N$, $38.5°W$; 3200 m a.s.l.). The core from 783 to 2282 m was drilled in 1991, and the lower section from 2280 m to bedrock was drilled in 1992. More information on the geographical environment of the station is available in the GRIP Members (1993) report. After drilling, the core was stored in a cold room at $-26°C$ at the University of Copenhagen, Denmark. Five GRIP ice-core segments, each 300–400 mm in length, were sent to Japan. After arrival in Japan they were stored in a cold room at $-50°C$.

The five ice segments are dated from 6.9 ka BP (1200.35–1200.65 m depth), 9.8 ka BP (1501.66–1502.05 m), 13.5 ka BP (1700.61–1700.91 m), 30.0 ka BP (2099.90–2100.20 m) and 43.1 ka BP (2300.65–2301.05 m) (Johnsen and others, 1997). The 6.9 and 9.8 ka BP sections belong to the Holocene. The 30.0 and 43.1 ka BP sections belong to the last glacial period. The 13.5 ka BP section belongs to Termination I. Ice samples of 40 mm length were sliced from the top of the 6.9 ka BP (1200.35–1200.39 m), 9.8 ka BP (1501.66–1501.70 m) and 13.5 ka BP (1700.61–1700.65 m) ice-core sections, and 50 mm long ice samples were sliced from the top of the 30.0 ka BP (2099.90–2099.95 m) and 43.1 ka BP (2300.65–2300.70 m) ice-core sections. These sub-cores were cut into three slices of exactly the same depth for analysis by optical microscopy, micro-Raman spectroscopy and ion chromatography.

2.1. Optical characterization

To measure the number and diameters of micro-inclusions, the ice was sliced with a microtome to a thickness of several millimeters and observed with an optical microscope (Olympus BH2-UMA, with objective lens Olympus ULWD Neo SPlan 50, numerical aperture (NA) 0.55, 50×) in a cold clean room at –15°C. According to the Becke test, the density contrast between micro-inclusions and the surrounding ice is strong enough to distinguish by optical microscopy. We cannot distinguish between dust (insoluble) and salt (water-soluble) inclusions, however, so both types are counted. Micro-inclusions with a diameter greater than 1.0 μm can be measured reliably by this method, but diameters less than 2.0 μm have a large margin of error. All micro-inclusions in the field of view ($0.14 \times 0.18 \times$ thickness mm^3) of the optical microscope were counted and measured, and we randomly picked 100 to calculate the average number per mm^3 and standard deviation. The density unit was calculated as count mL^{-1} from count mm^{-3}. In addition to measurements to compare the different spatial distribution of micro-inclusions in 6.9 ka BP (Holocene) and 30.0 ka BP (last glacial period) ice, micro-inclusions were measured in the field of the microscope ($0.14 \times 0.18 \times$ thickness mm^3), and 100 views were measured to construct a view of $1.4 \times 1.8 \times$ thickness mm^3. To measure the spatial distribution, we selected one view ($1.4 \times 1.8 \times$ thickness mm^3) which contains a grain boundary and air hydrate, but does not include the plate-like inclusions, because we cannot see the micro-inclusions in plate-like inclusions. In these observations, we have not accounted for a possible influence of seasonal variability on the differences between samples taken from different time periods (GRIP Members, 1993).

2.2. Micro-Raman spectroscopy

To measure the chemical composition of the inclusions, we used micro-Raman spectroscopy within a cold chamber controlled to –30°C by N_2 gas flow. The micro-Raman spectroscope uses a triple monochromator (Jobin-Yvon, T64000) equipped with a charge-coupled device (CCD) detector. The CCD detector has good quantum efficiency from 500 to 900 nm. We employed a laser beam of wavelength 514.5 nm and power 20 mW. We chose an objective lens with a long working distance, 6 mm focal length and NA 0.75 (Mitutoyo, M Plan Apo 100×). The absolute frequency of the monochromator was calibrated using a neon emission line. The resolution of the Raman spectrum was 0.6 cm^{-1}.

We measured reference spectra for various salts in advance. The characteristic features of Raman spectra have been recognized in previous works (e.g. Socrates, 2001). For instance, SO_4^{2-} produces a strong band at 955–1065 cm^{-1} from the S-O symmetric stretching mode. Its other modes give rise to medium–strong bands at 405–530, 580–680, 1080–1130 and 1140–1200 cm^{-1}. NO_3^- has a strong band at 1015–1070 cm^{-1} and a medium–weak band at 700–770 cm^{-1}. CO_3^{2-} has a medium–strong band at 1020–1100 cm^{-1} and a weak band at 670–745 cm^{-1}. $CaCO_3$, a key compound of many inclusions, has a strong band at 1085 cm^{-1}. Details on the reference specimens prepared for these sulfate and nitrate salts and acid solutions have been given in a previous study (Ohno and others, 2005).

2.3. SEM-EDS

SEM-EDS analysis determines which chemical elements are present in the micro-inclusions, information that can be used to deduce the chemical compounds. This analysis was performed using a JSM-6360LV (Japan Electron Optics Ltd (JEOL)) SEM system and a JED2201 (JEOL) EDS system. The accelerating voltage of the SEM was 15 keV. The apparatus included an optical probe (Renishaw) to observe the surface of the ice samples. Cores of 5.2 mm diameter were extracted from the 6.9 ka BP (1200.40 m) and 30.0 ka BP (2099.96 m) sections using a trephine drill (Nobel Biocare). The bases of these specimens were cut down to a height of 3–4 mm using a microtome. Each specimen was put into a stainless-steel holder of diameter 5.3 mm and depth 2.5–3.0 mm, held in place with a screw. The sample was kept in an Alto2100 (Gatan) cryo-system during analysis. Inside the SEM chamber, the specimen was sublimated at –90°C until micro-inclusions were exposed on the ice surface. The sublimation rate was about 2 μm min^{-1} under these conditions. The specimen was maintained at –135°C for the remainder of the analysis.

2.4. Ion chromatography

Ion chromatography is one of the most common methods of measuring the ionic species present in ice. We decontaminated the ice samples used for ion chromatography by cutting away the surface with a clean ceramic knife, on a clean bench in a clean cold room at –15°C. The decontaminated ice samples were immediately sealed in a clean polyethylene bag. After melting in its bag outside the cold room, the ice sample was passed through a filter with 0.45 μm pores and analyzed in a Dionex 500 chromatograph. We measured the concentrations of sodium, magnesium, calcium, chloride, nitrate and sulfate ions. To test for possible contamination, we measured ultra-pure water using the same methods and found no peaks in the chromatograph spectrum. The process of sample preparation has been described in detail by Iizuka and others (2006).

To determine the calcium ion concentration due to micro-inclusions, for each sample we also calculated the total volume of inclusions containing $CaSO_4 \cdot 2H_2O$ and $CaCO_3$, based on the size distribution curve (Fig. 1) and the observed proportion of micro-inclusions of this type (Fig. 5). The calculated calcium ion is shown in Table 1 as $_{calc.}Ca^{2+}$. The difference between the calcium ion concentration found by ion chromatography and that estimated from micro-inclusions of calcium salts is considered in section 4.

3. RESULTS

3.1. Number density and diameter of micro-inclusions

The number densities, n (mL^{-1}), and mean diameters, d (μm), of the micro-inclusions found in each sample are shown in Table 1. The number density of micro-inclusions is more than an order of magnitude lower in the Holocene than in the glacial period. The mean diameter of the micro-inclusions is about the same at each depth. The diameter distributions for each climate period are shown in Figure 1. The overall shape of the distribution is the same in each period, in that the percentage of micro-inclusions decreases with increasing diameter. The shapes of these distributions correspond well to the size distribution curves of larger dust particles (Steffensen, 1997), except for the outstanding abundance of 2.0–2.5 μm inclusions in Holocene ice. This similarity suggests that water-soluble micro-inclusions smaller than 2.0 μm may have a distribution similar to that of dust. The excess of 2.0–2.5 μm inclusions remains to be explained, but it seems likely that water-soluble compounds are responsible.

To illustrate the spatial distribution of micro-inclusions, including both dust and water-soluble compounds, Figure 2 shows the micro-inclusions, clathrate hydrates, air bubbles and grain boundaries observed in two samples of 6.9 and 30.0 ka BP ice. Note that the micro-inclusions are not distributed uniformly in either sample; they tend to be found in tight groups. Previous research has postulated that the water-soluble impurities used as climate proxies are influenced by diffusion through a vein network (e.g. Rempel and others, 2001). If the water-soluble impurities exist as liquid phase, these may diffuse through a vein network. However, we find that most of the micro-inclusions (water-soluble and dust) are distributed in the ice grain at these depths, and chemical compositions of water-soluble micro-inclusions are measured by micro-Raman spectroscopy.

3.2. Micro-Raman spectroscopy

In the Raman spectra of the micro-inclusions we found several sharp peaks. We compare these data to the
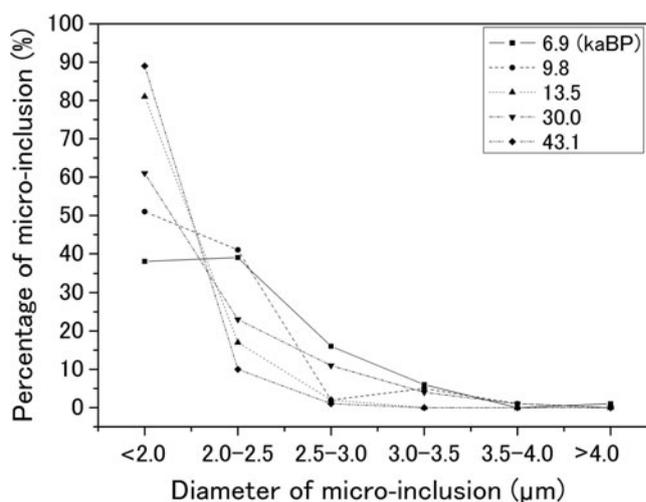

Fig. 1. Percentage of micro-inclusions in six diameter ranges. Inclusions of less than 2.0 μm diameter are merged into a single bin because their sizes have a large uncertainty. Inclusions of diameter greater than 4.0 μm are merged because they are rare.

reference spectra of pure specimens. Below, we focus on $CaSO_4 \cdot 2H_2O$ and $CaCO_3$, because calcium is the most abundant ion in GRIP ice.

Calcium sulfate ($CaSO_4 \cdot 2H_2O$)

In some inclusions, a sharp primary peak is detected at 1009.05 cm^{-1} with sub-peaks at 215.35, 414.23, 493.04, 620.75 and 670.22 cm^{-1} (Fig. 3c and g). Inclusions of this type were found at all five depths. The reference spectrum for $CaSO_4 \cdot 2H_2O$ has its main peak at 1007.84 cm^{-1} (from the S-O symmetric stretching mode) and secondary peaks at 216.75, 413.60, 493.07, 620.78 and 670.25 cm^{-1} from other modes (Fig. 3b and f). The two Raman spectra correspond very well. Note that the 215.34 and 216.75 cm^{-1} peaks (Fig. 3f and g) come from the ice itself (Fig. 3a), as shown in Figure 3a and c. This analysis thus confirms the existence of $CaSO_4 \cdot 2H_2O$ in the GRIP ice core.

Table 1. Micro-inclusion counts and ion concentrations in the five GRIP ice-core sections. N is the total number of micro-inclusions found by optical microscope in all 100 views (i.e. the whole $1.8 \times 1.4 \times$ thickness mm^3 sample, where one view is $0.80 \times 0.14 \times$ thickness mm^3); the number of inclusions measured using Raman spectroscopy is given in parentheses. n is the number density of micro-inclusions in the sample volume. d is the mean diameter of the micro-inclusions. The thicknesses of the ice sections are also shown; the number in parentheses is the thickness of the section which was re-sliced by microtome at the time the spatial distribution was measured, following measurement of the number density and mean diameter of the micro-inclusions. The ion concentrations measured at each depth are averaged over five samples, $_{calc.}Ca^{2+}$ is calculated from the diameter and number density of $CaSO_4 \cdot 2H_2O$ and $CaCO_3$. The sum of the two major anion concentrations ($NO_3^- + SO_4^{2-}$) is also given

| Depth	Period		N	n	d	Thickness	Cl$^-$	NO$_3^-$	SO$_4^{2-}$	Na$^+$	Mg^{2+}	Ca^{2+} ($_{calc.}$Ca^{2+})	NO$_3^-$ + SO$_4^{2-}$
m		ka BP		mL^{-1}	μm	mm	μEq L^{-1}	μEq L^{-1}	μEq L^{-1}	μEq L^{-1}	μEq L^{-1}	μEq L^{-1}	μEq L^{-1}
1200.35–1200.39	Holocene	6.9	14 (50)	$(0.06 \pm 0.01) \times 10^5$	2.15 ± 0.49	3.3 (1.4)	0.66	0.99	0.59	1.08	0.14	0.58 (0.13)	1.58
1501.66–1501.70	Holocene	9.8	28 (95)	$(0.12 \pm 0.03) \times 10^5$	2.05 ± 0.45	2.8	0.94	1.23	1.44	0.91	0.24	0.70 (0.15)	2.67
1700.61–1700.65	Termination I	13.5	200 (43)	$(0.85 \pm 0.09) \times 10^5$	1.74 ± 0.31	5.0	1.16	1.19	1.20	1.06	0.36	1.84 (1.37)	2.40
2099.90–2099.95	Last Glacial Period	30.0	1017 (80)	$(4.3 \pm 0.5) \times 10^5$	2.03 ± 0.47	2.0 (1.65)	1.99	0.93	2.05	1.76	1.03	7.17 (4.89) [0.55]	2.98
2300.65–2300.70	Last Glacial Period	43.1	500 (61)	$(2.1 \pm 0.4) \times 10^5$	1.72 ± 0.24	2.0	1.32	1.14	1.02	1.23	0.51	1.97 (1.92)	2.16
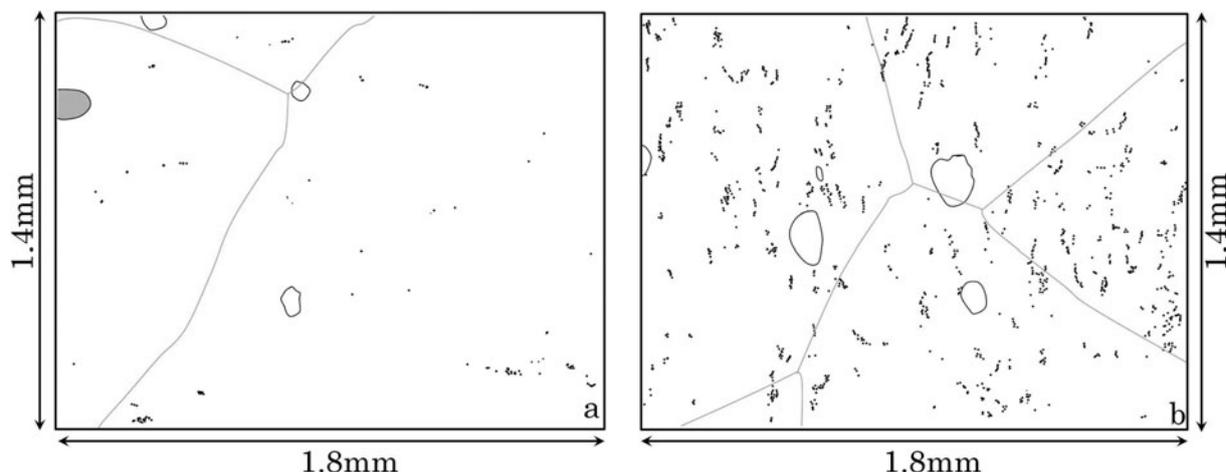
Fig. 2. Spatial distribution of micro-inclusions (black dots), clathrate hydrates (white regions), an air bubble (gray region) and grain boundaries (solid lines) in ice: (a) a 1.4 mm × 1.8 mm × 1.4 mm thick section of 6.9 ka BP ice; (b) a similar section (1.65 mm thick) of 30.0 ka BP ice.

Calcium carbonate (CaCO$_3$)
In the 30.0 ka BP ice, some inclusions show a sharp primary peak at 1085.74 cm^{-1} with sub-peaks at 215.38, 282.34 and 711.70 cm^{-1} (Fig. 3e and i). The reference spectrum of CaCO$_3$ has its main peak at 1085.74 cm^{-1}, probably from

the C-O symmetric stretching mode, and two sub-peaks at 281.66 and 712.34 cm^{-1} (Fig. 3d and h). Note that the 215.38 cm^{-1} (Fig. 3i) peak comes from the ice itself (Fig. 3a). The observed spectra thus clearly indicate the presence of CaCO$_3$ in the GRIP ice core (Fig. 3d, e, h and i).

3.3. SEM-EDS

Micro-inclusions exposed by sublimation inside the SEM chamber (as described in section 2) were measured by EDS. SEM images of micro-inclusions found in the 6.9 and 30.0 ka BP ice are shown in Figure 4d and e respectively. X-ray spectra of three micro-inclusions observed in the 6.9 and 30.0 ka BP ice samples are shown in Figure 4a, b and c respectively. In the 6.9 ka BP samples (Fig. 4a, b and d) both S and Ca were identified. An abundance of O was also measured, which mainly comes from ice. Micro-inclusions having both S and Ca turned out to be CaSO$_4$·2H$_2$O. In the 30.0 ka BP sample, the micro-inclusion contains C, O and Ca (Fig. 4c and e). Such inclusions most likely consist of CaCO$_3$. The results of SEM-EDS analysis therefore support the Raman spectroscopy identification of CaSO$_4$·2H$_2$O and CaCO$_3$.

Taking the micro-Raman spectroscopy and SEM-EDS results together, we claim the first direct evidence that CaSO$_4$·2H$_2$O and CaCO$_3$ exist as solid-phase micro-inclusions in the GRIP ice core.

3.4. Ion chromatography

To further support the above results, we measured the concentrations of sodium, magnesium, calcium, chloride, nitrate and sulfate ions in the same ice sections by ion chromatography (Table 1). In Holocene ice, we find fewer calcium ions than sulfate and nitrate ions: 0.58 vs 1.58 μEq L^{-1} at 6.9 ka BP and 0.70 vs 2.67 μEq L^{-1} at 9.8 ka BP, where the second value is the total concentration of (NO$_3^-$ + SO$_4^{2-}$). On the other hand, in the 30.0 ka BP section, we find a significant excess of calcium ions (7.17 μEq L^{-1}) compared to the sulfate and nitrate ions (totaling 2.98 μEq L^{-1}). The 43.1 ka BP ice has a more modest excess of calcium ions (1.97 μEq L^{-1}) with respect to sulfate and nitrate ions (2.16 μEq L^{-1}).

These results can support a discussion of the chemical compounds present in ice (Iizuka and others, 2008). The ion balance observed in Holocene ice (6.9 and 9.8 ka BP)
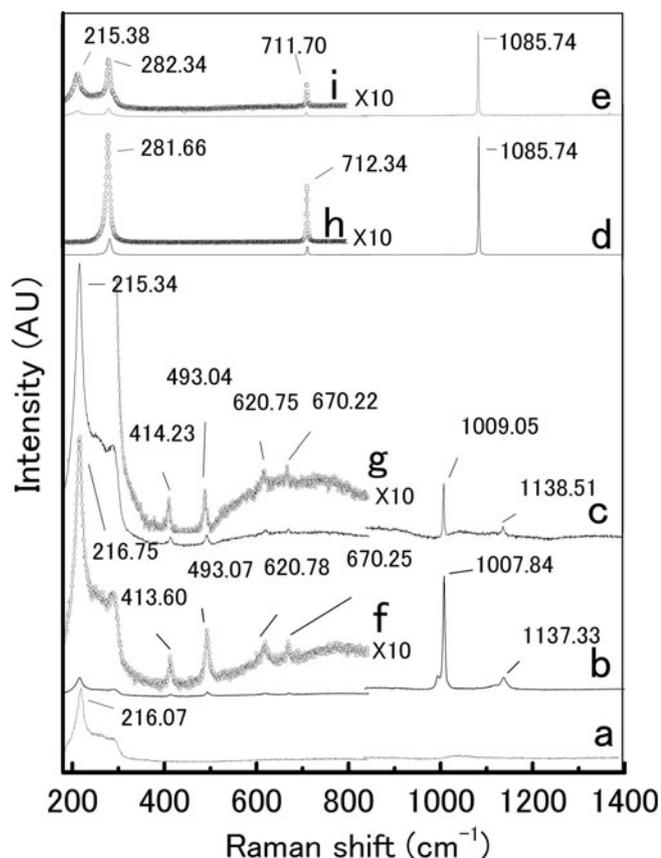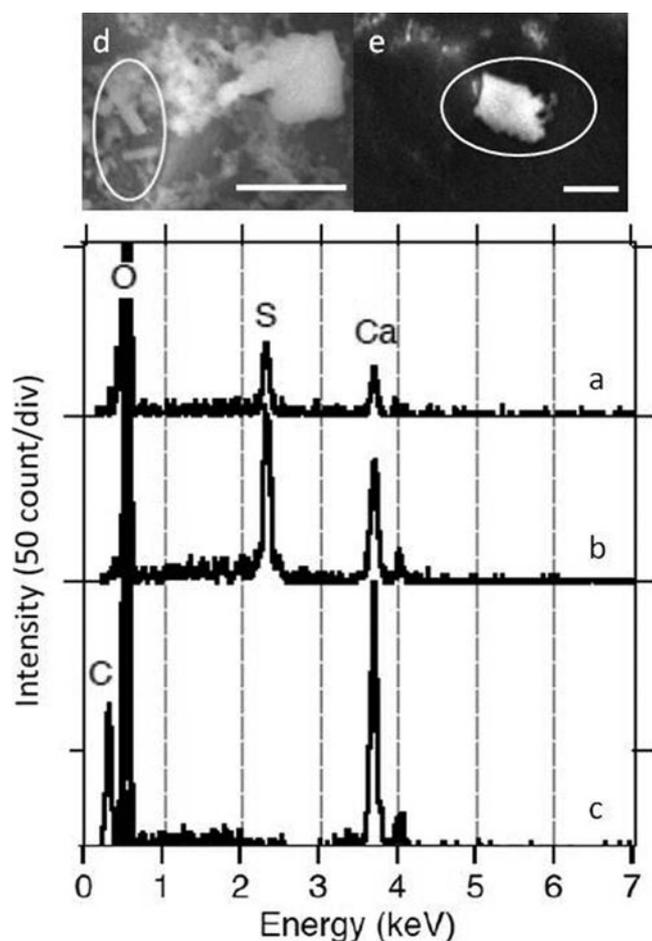

Fig. 3. Raman spectra (signal intensity in arbitrary units (AU)) of reference specimens and the measured micro-inclusions. a. GRIP ice without inclusions; b. pure specimen of CaSO$_4$·2H$_2$O in ice prepared with ultra-pure water; c. CaSO$_4$·2H$_2$O inclusion found in the GRIP ice core (the spectrum is from 9.8 ka BP); d. pure specimen of CaCO$_3$; e. CaCO$_3$ inclusion found in 30.0 ka BP ice from the GRIP core. Curves f–i are magnifications (10×) of spectra b–e respectively, from 180 to 850 cm^{-1}.

Fig. 4. (a–c) X-ray spectra of micro-inclusions found in (a) 6.9 ka BP ice and (b, c) 30.0 ka BP ice. Inclusions (a) and (b) are deduced to be $CaSO_4 \cdot 2H_2O$ (containing oxygen, sulfur and calcium). Inclusion (c) is deduced to be $CaCO_3$ (containing oxygen, carbon and calcium). (d, e) Pictures of the inclusions yielding spectra (a) and (c) respectively.

Fig. 5. Number of micro-inclusions identified as containing various compounds in the GRIP ice core. $CaSO_4 \cdot 2H_2O$ is a major compound at all depths. $Na_2SO_4 \cdot 10H_2O$ and $MgSO_4 \cdot 11H_2O$ are difficult to distinguish (Ohno and others, 2005, 2006). $CaCO_3$ is found only in the 30.0 ka BP ice. Nitrate and quartz are also present, and classified in the 'other' category along with some spectra which have not yet been identified. Inclusions for which no spectral features other than those of ice could be detected are classified as 'no Raman signal'.

suggests that the calcium ion could exist as both $CaSO_4 \cdot 2H_2O$ and calcium nitrate. In the 30.0 ka BP ice, the excess of calcium ions strongly suggests the presence of $CaCO_3$. In the 43.1 ka BP ice, a more modest excess of calcium ions suggests that a small amount of $CaCO_3$ should have remained. Although the existence of these compounds is inferred, the results support the findings of micro-Raman spectroscopy and SEM-EDS analysis. Note, however, that we did not find direct evidence of $CaCO_3$ in the 43.1 ka BP ice over the course of this analysis. This section must therefore have significantly less $CaCO_3$ than the 30.0 ka BP section. Analysis of more inclusions would probably reveal some, but the process is very time-consuming.

3.5. Micro-inclusions identified by Raman spectroscopy

The number of micro-inclusions measured by Raman spectroscopy is given in Table 1. The number density includes both water-soluble and water-insoluble inclusions, as shown in Figure 5. Among water-soluble inclusions, we expect to find sulfate, nitrate and chloride salts given the results of ion chromatography (see section 3.4 and Table 1). As our earlier measurements of reference chemical compounds demonstrate, both sulfate and carbonate salts have strong symmetric stretching modes (S-O and C-O
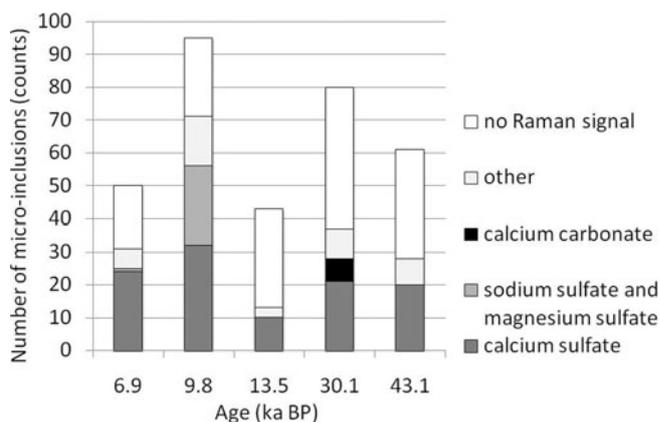
respectively). The nitrate salt also has a symmetric (N-O) stretching mode, but its response is relatively weak. We therefore could not find direct evidence for nitrate salts in the ice via Raman spectroscopy in this study. Chloride salts (e.g. $NaCl \cdot 2H_2O$) can be identified by their hydrate (O-H) vibration mode in the range $3100–3600\,cm^{-1}$ (Dubessy and others, 1982), but this signal may be hidden by the O-H vibration of ice in this measurement.

A few water-insoluble micro-inclusions (e.g. dust) were partly identified by their chemical compounds, while others could not be matched to reference spectra. The latter are classified as 'other' in Figure 5. Micro-inclusions with no Raman peaks except for the ice background are classified as 'undetectable', although they may well possess a weak signal hidden by the ice. For all the reasons given above, only water-soluble inclusions containing sulfate and carbonate salts could be clearly identified by this method.

Figure 5 shows that $CaSO_4 \cdot 2H_2O$ exists not just in glacial period ice but also in Holocene ice. On the other hand, $Na_2SO_4 \cdot 10H_2O$ and $MgSO_4 \cdot 11H_2O$ were found only in Holocene ice sections (6.9 and 9.8 ka BP). The Raman spectra of $Na_2SO_4 \cdot 10H_2O$ and $MgSO_4 \cdot 11H_2O$ are difficult to distinguish from one another, because the molecules have very similar stretching modes. These sulfate salts have been discussed in two of our previous papers (Ohno and others, 2005, 2006). We found $CaCO_3$ in the 30.0 ka BP ice section, but could not find it in the 43.1 ka BP ice section. As the ion-chromatography results suggest, the amount of $CaCO_3$ in the latter section is probably too small to measure easily (Table 1).

4. DISCUSSION

This study provides the first direct evidence that calcium sulfate ($CaSO_4 \cdot 2H_2O$) and $CaCO_3$ exist in solid form in the Greenland ice core, using micro-Raman spectroscopy and SEM-EDS analysis of individual inclusions to support the results of ion chromatography. The existence of $CaCO_3$ and $CaSO_4 \cdot 2H_2O$ in the Greenland ice core has previously been

inferred from ion chromatography (Mayewski and others, 1994; Legrand and others, 1997), and the existence of carbonate has previously been deduced by SEM-EDS (Laj and others, 1997; Maggi, 1997). Our own findings confirm the existence of both $CaCO_3$ and $CaSO_4 \cdot 2H_2O$ in GRIP ice. Sala and others (2008) showed by Raman spectroscopy that three types of calcium carbonate are found in the shallow ice of the Antarctic ice sheet (i.e. $CaCO_3$, $CaCO_3 \cdot 2H_2O$ and $CaCO_3 \cdot 6H_2O$). They can be distinguished very clearly by micro-Raman spectroscopy. In this study, we could not find calcium carbonates except $CaCO_3$. We now discuss how ion concentrations can be estimated from the abundance of salt inclusions, the significance of excess carbon dioxide from $CaCO_3$, and the paleoclimatological impact of these results.

4.1. Ion-concentration estimates based on micro-inclusion volume

To determine the proportion of calcium ions originating from $CaSO_4 \cdot 2H_2O$ and $CaCO_3$ in the form of micro-inclusions, we estimated the total mass of such inclusions in the ice section (see section 2.4). Because it is difficult to measure the particle volume, we treat all inclusions as spheres. In ice from the glacial period and Termination I, it is clear that $CaSO_4 \cdot 2H_2O$ inclusions (and $CaCO_3$, especially in the 30.0 ka BP section) make the most important contribution. The calcium ion abundance calculated from micro-inclusions is comparable to that measured by ion chromatography (Table 1): at least 74%, 68% and 98% of calcium ions can be attributed to $CaSO_4 \cdot 2H_2O$ in the 13.5, 30.0 and 43.1 ka BP samples respectively. At least 8% of calcium ions come from $CaCO_3$ in the 30.0 ka BP sample. In Holocene ice, on the other hand, $CaSO_4 \cdot 2H_2O$ contributes only 22% and 21% of calcium ions in the 6.9 and 9.8 ka BP sections respectively. The remaining ions probably come from other salts.

4.2. Significance of carbon dioxide

The amount of $CaCO_3$ deduced to exist in the ice is sensitive to the measuring method. Anklin and others (1995) compared two CO_2 measurements in GRIP ice, obtained by melting–refreezing and dry extraction. In the first method, $CaCO_3$ dissolves in the melted ice and probably reacts with acid in solution. This produces more CO_2 than would be observed in a dry extraction process. The excess CO_2 can be calculated from the chemical reaction, written as

$$CaCO_3 + 2H^+ \rightarrow Ca^{2+} + excess CO_2 + H_2O. \qquad (1)$$
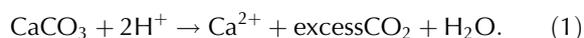
This formula implies that 1 mol of $CaCO_3$ produces 1 mol of excess CO_2 and 1 mol of Ca^{2+}. We measured $0.28\,\mu mol\,L^{-1}$ $(0.55\,\mu Eq\,L^{-1})$ of Ca^{2+} in the form of $CaCO_3$, so only $0.28\,\mu mol\,L^{-1}$ (12.19 ppb) of excess CO_2 could be produced from our observed number density of $CaCO_3$. This cannot explain the observed excess of CO_2 that Anklin and others (1995, 1997) suggested. This difference appears to suggest that we should have found more $CaCO_3$ in the 30.0 ka BP ice by Raman spectroscopy. Heterogeneous chemical reactions that take place during measurement might also have been active in the ice sheet and/or atmosphere when the layer was formed.

4.3. Significance of sulfate and carbonate salts

Equation (1) is strongly dependent on the acidity of the ice. For the GRIP ice core, this quantity has already been determined by electrical conductivity measurement (ECM) (Wolff and others, 1995, 1997). In Holocene ice the

existence of acid leads to the chemical reaction, whereby HCl may sublimate from reactant,

$$2NaCl + H_2SO_4 \rightarrow Na_2SO_4 + 2HCl, \qquad (2)$$

which supports our finding of the existence of $Na_2SO_4 \cdot 10H_2O$ and $MgSO_4 \cdot 11H_2O$ in Holocene ice. In contrast, less acidity is expected in the glacial period ice due to the presence of $CaCO_3$.

The existence of sulfates and carbonates in the atmosphere is related to the radiative forcing process. Jarzembski and others (2003) showed that sulfate and carbonate salts have significantly different refractive indices of absorption from ultraviolet to infrared. The origins of calcium ions in various climate conditions have been previously discussed by several authors (Mayewski and others, 1994; De Angelis and others, 1997; Laj and others, 1997; Legrand and others, 1997; Svensson and others, 2000). A study of Sr and Nd isotopic compounds and rare-earth concentrations suggests that eastern Asia was the main source of dust (including calcium ions) during the last glacial period (Svensson and others, 2000). With respect to the Holocene, Dibb and others (2007) found that most aerosols came from Asia and the Sahara Desert. These studies suggest that sulfate and carbonate were transported by the atmosphere from Asia and/or the Sahara Desert to the Greenland ice sheet.

It is still necessary to clarify which chemical reactions occurred during formation of the ice sheet, as well as quantifying their rates. Achieving this understanding will allow the paleoclimatology community to discuss how the radiative forcing of aerosols occurred in detail.

5. CONCLUSION

This study has measured the chemical composition, size distribution and spatial distribution of micron-scale inclusions in the GRIP ice core. We find direct evidence for calcium sulfate ($CaSO_4 \cdot 2H_2O$) and calcium carbonate ($CaCO_3$) in some inclusions by employing Raman spectroscopy and SEM-EDS. $CaSO_4 \cdot 2H_2O$ is the major water-soluble compound, but a large amount of $CaCO_3$ also exists in the glacial period ice. The latter result is supported by the high concentration of calcium ions observed using ion chromatography. The size distribution curves of the micro-inclusions, which include both water-soluble and water-insoluble types, correspond well with previously reported size distribution curves of dust particles (Steffensen, 1997). The micro-inclusions also tend to group together in small clusters, rather than being evenly distributed in the ice grains. These measurements indicate that water-soluble impurities existing as micro-inclusions could be preserved in the depth profile, serving as reliable proxies of past climate.

REFERENCES

Anklin, M., J.M. Barnola, J. Schwander, B. Stauffer and D. Raynaud. 1995. Processes affecting the CO_2 concentrations measured in Greenland ice. *Tellus,* **47B**(4), 461–470.

Anklin, M. *and 6 others*. 1997. CO_2 record between 40 and 8 kyr B.P. from the Greenland Ice Core Project ice core. *J. Geophys. Res.,* **102**(C12), 26,539–26,546.

De Angelis, M., J.P. Steffensen, M. Legrand, H. Clausen and C. Hammer. 1997. Primary aerosol (sea salt and soil dust) deposited in Greenland ice during the last climatic cycle: comparison with East Antarctic records. *J. Geophys. Res.,* **102**(C12), 26,681–26,698.

Dibb, J.E., S.I. Whitlow and M. Arsenault. 2007. Seasonal variations in the soluble ion content of snow at Summit, Greenland: constraints from three years of daily surface snow samples. *Atmos. Environ.,* **41**(24), 5007–5019.

Dubessy, J., D. Audeoud, R. Wilkins and C. Kosztolanyi. 1982. The use of the Raman microprobe MOLE in the determination of the electrolytes dissolved in the aqueous phase of fluid inclusions. *Chemical Geol.,* **37**(1–2), 137–150.

Genceli, F.E., A.L. Lutz, A.L. Spek and G.-J. Witkamp. 2007. Crystallization and characterization of a new magnesium sulphate $MgSO_4 \cdot 11H_2O$. *Cryst. Growth Des.,* **7**(12), 2460–2466.

Greenland Ice-Core Project (GRIP) Members. 1993. Climate instability during the last interglacial period recorded in the GRIP ice core. *Nature,* **364**(6434), 203–207.

Iizuka, Y., T. Hondoh and Y. Fujii. 2006. Na_2SO_4 and $MgSO_4$ salts during the Holocene period derived by high-resolution depth analysis of a Dome Fuji ice core. *J. Glaciol.,* **52**(176), 58–64.

Iizuka, Y. *and 6 others*. 2008. A relationship between ion balance and the chemical compounds of salt inclusions found in the Greenland Ice Core Project and Dome Fuji ice cores. *J. Geophys. Res.,* **113**(D7), D07303. (10.1029/2007JD009018.)

Jarzembski, M.A., M.L. Norman, K.A. Fuller, V. Srivastava and D.R. Cutten. 2003. Complex refractive index of ammonium nitrate in the 2–20-µm spectral range. *Appl. Opt.,* **42**(6), 922–930.

Johnsen, S.J., D. Dahl-Jensen, W. Dansgaard and N.S. Gundestrup. 1995. Greenland paleotemperatures derived from GRIP bore-hole temperature and ice core isotope profiles. *Tellus,* **47B**(5), 624–629.

Johnsen, S.J. *and 14 others*. 1997. The $\delta^{18}O$ record along the Greenland Ice Core Project deep ice core and the problem of possible Eemian climatic instability. *J. Geophys. Res.,* **102**(C12), 26,397–26,410.

Kargel, J.S. 1991. Brine volcanism and the interior structures of asteroids and icy satellites. *Icarus,* **94**(2), 368–390.

Laj, P. *and 7 others*. 1997. Distribution of Ca, Fe, K, and S between soluble and insoluble material in the Greenland Ice Core Project ice core. *J. Geophys. Res.,* **102**(C12), 26,615–26,623.

Legrand, M. *and 6 others*. 1997. Sulfur-containing species (methanesulfonate and SO_4) over the last climatic cycle in the Greenland Ice Core Project (central Greenland) ice core. *J. Geophys. Res.,* **102**(C12), 26,663–26,679.

Maggi, V. 1997. Mineralogy of atmospheric microparticles deposited along the Greenland Ice Core Project ice core. *J. Geophys. Res.,* **102**(C12), 26,725–26,734.

Mayewski, P.A. *and 13 others*. 1994. Changes in atmospheric circulation and ocean ice cover over the North Atlantic during the last 41,000 years. *Science,* **263**(5154), 1747–1751.

Mulvaney, R., E.W. Wolff and K. Oates. 1988. Sulphuric acid at grain boundaries in Antarctic ice. *Nature,* **331**(6153), 247–249.

Ohno, H., A. Igarashi and T. Hondoh. 2005. Salt inclusions in polar ice core, location and chemical form of water-soluble impurities. *Earth Planet. Sci. Lett.,* **232**(1–2), 171–178.

Ohno, H., M. Igarashi and T. Hondoh. 2006. Characteristics of salt inclusions in polar ice from Dome Fuji, East Antarctica. *Geophys. Res. Lett.,* **33**(8), L08501. (10.1029/2006GL025774.)

Rempel, A.W., E.D. Waddington, J.S. Wettlaufer and M.G. Worster. 2001. Possible displacement of the climate signal in ancient ice by premelting and anomalous diffusion. *Nature,* **411**(6837), 568–571.

Sala, M. *and 10 others*. 2008. Evidence of calcium carbonates in coastal (Talos Dome and Ross Sea area) East Antarctica snow and firn: environmental and climatic implications. *Earth Planet. Sci. Lett.,* **271**(1–4), 43–52.

Socrates, G. 2001. *Infrared and Raman characteristic group frequencies: tables and charts. Third edition*. Chichester, John Wiley & Sons.

Steffensen, J.P. 1997. The size distribution of microparticles from selected segments of the GRIP ice core representing different climatic periods. *J. Geophys. Res.,* **102**(C12), 26,755–26,763.

Svensson, A., P.E. Biscaye and F.E. Grousset. 2000. Characterization of late glacial continental dust in the Greenland Ice Core Project ice core. *J. Geophys. Res.,* **105**(D4), 4637–4656.

Usdowski, E. and M. Dietzel. 1998. *Atlas and data of solid-solution equilibria of marine evaporites*. Berlin, etc., Springer-Verlag.

Wolff, E.W., J.C. Moore, H.B. Clausen, C.U. Hammer, J. Kipfstuhl and K. Fuhrer. 1995. Long-term changes in the acid and salt concentrations of the Greenland Ice Core Project ice core from electrical stratigraphy. *J. Geophys. Res.,* **100**(D8), 16,249–16,263.

Wolff, E.W., J.C. Moore, H.B. Clausen and C.U. Hammer. 1997. Climatic implication of background acidity and other chemistry derived from electrical studies of the Greenland Ice Core Project ice core. *J. Geophys. Res.,* **102**(C12), 26,325–26,332.